Electrochemical and Microscopic Study on Corrosion Characteristics of Cement-Mortar-Lined Ductile Iron Pipe in Flowing Solutions

Xiang-Nan Li, Xiao-Bao Zuo[*], *Shuai Zou, Yu-Xiao Zou*

Department of Civil Engineering, School of Science, Nanjing University of Science & Technology, Nanjing, 210094, P.R.China
[*]E-mail: xbzuo@sina.com

Corrosion characteristics of ductile iron (DI) pipe specimen lined cement mortar (CM) layer were investigated by the electrochemical and microscopic analysis when placed in flowing purified water, 6M NH_4NO_3 solution and 6M NH_4Cl solution for 120 days, respectively. Electrochemical characteristics of specimen were evaluated by OCP, PDP and EIS. Meanwhile, the microstructural morphology and phase composition of leached CM lining and corroded CM-DI interfacial zone in the specimen were characterized by SEM/EDS and XRD. Results show that, the CM lining and DI surface of specimen have different corrosion characteristics in three flowing solutions, and the specimen in flowing purified water has basically no leaching of CM lining and corrosion of CM-DI interfacial zone. But, there are obvious leaching of the CM lining and no corrosion of CM-DI interfacial zone of specimen in flowing NH_4NO_3 solution. However, severe corrosion occurs on the CM lining and DI surface of the specimen in flowing NH_4Cl solution for 120 days.

1. INTRODUCTION

Ductile iron (DI) pipe lined with cement-mortar (CM) has been widely used in water supply and drainage engineering, because of its large diameter, high bearing capacity and good durability when deeply buried underground [1,2]. The cement-mortar protection layer can protect DI pipe from direct corrosion of flowing water and reduce the friction between flowing water and inner wall of pipe [3]. Meanwhile, pore solution with a high alkalinity produced by the hydration of cement in mortar is helpful for the passivation of DI surface, which can enhance the protective effect of CM lining on DI pipe [4]. However, long-termly in water supply engineering, cement mortar lining is easily subjected to the leaching caused by the flowing water [5], which results in a gradual decrease in the protective effect of

CM lining on DI, finally causing a corroded failure of DI pipe [6]. Thus, the corrosion of DI pipe induced by the long-term flowing water has a significant impact on the durability of cement-mortar-lined ductile iron (CMLDI) pipe, the study of which is necessary for the material design of CM lining and lifetime evaluation of CMLDI pipe in water supply [7].

The durability problem of CMLDI pipe served in water supply mainly involves two aspects [8]: the leaching of CM lining and corrosion of DI surface. In water supply engineering, the flowing water with low calcium content, like the desalinated sea water and tap water, usually causes the dissolution of cement-hydrated products, such as calcium hydroxide (CH) and hydrated calcium silicate(C-S-H) gel [9]. This dissolution can deteriorate the microstructure of CM lining, decrease the alkalinity of pore solution, and increase the porosity of cement mortar [10]. The decrease of pore solution's alkalinity will reduce the chloride threshold, which can cause a premature corrosion of ductile iron [7]. In addition, the increase of porosity and deterioration of microstructure further accelerate the calcium and chloride diffusion in cement mortar as well as the corrosion of DI pipe in flowing water [11]. Similar to reinforced concrete in chloride environments, the volumetric expansion caused by rusted production at the interfacial zone between CM and DI results in the crack and damage CM lining, also influencing the calcium and chloride diffusion. Thus, the durability deterioration of CMLDI pipe is a complicated interaction process between the leaching of CM lining and corrosion of DI pipe, which can shorten the in-service lifetime of the CMLDI pipe in water supply.

At present, the studies of CMLDI pipe mainly focus on the effects of CM materials on the supplied water quality for its engineering applications as well as the passivation of DI surface in simulated pore solution of CM [12,13], but the corrosion characteristics or durability deterioration of the CMLDI pipe exposed to flowing water has not attracted enough attention. Electrochemical measurement, such as electrochemical impedance spectroscopy (EIS), is a suitable technique to investigate the corrosion behavior of CM materials and metal surface like steel and DI [14]. Based on the analysis of equivalent circuits associated with the EIS diagram, the electrochemical parameters, including open circuit potential, polarization resistance and corrosion current density, are acquired to survey the corrosion process of steel or DI covered with CM materials [15]. In addition, the corrosion process of CM materials and metal surface can also be characterized by their microstructure and physico-chemical properties. Microscopic analysis, such as scanning electron microscopy (SEM) and X-ray diffraction (XRD) analysis, can directly investigate the properties of corrosion production formed on the metal surface and the covered CM materials, including its microstructure and composition [16]. Thus, the experimental investigation on the electrochemical and physico-chemical properties of the interfacial zone between CM and DI of the CMLDI pipe can be helpful to reveal its corrosion-resistance mechanism.

In order to study the deterioration mechanism of CMLDI pipe in flowing water, some specimens of DI pipe lined with CM were prepared, and then they were respectively immersed in different corrosive solutions, including purified water, 6M ammonium nitrate solution and 6M ammonium chloride solution, which were disturbed by a pump with 12 watts to simulate flowing water. Electrochemical measurements were performed to study the corrosion characteristics of specimens in flowing corrosive solutions, and their electrochemical characteristics were evaluated by open circuit potential (OCP), potentiodynamic polarization (PDP) and electrochemical impedance spectra (EIS). Simultaneously, the

chemical composition and microscopic morphology of both CM lining and DI surface of CMLDI specimens in different flowing solutions were analyzed by means of X-ray diffraction (XRD) and scanning electron microscopy (SEM) together with Energy Dispersive X-ray Spectroscopy (EDS).

2. EXPERIMENTS

2.1 Materials

The cement used in the experiment is the 52.5-grade ordinary Portland cement, and its chemical composition is listed in Table 1. The density of cement is $3150 kg/m^3$, and its specific surface area is 369.6 m^2/kg. The fineness modulus and apparent density of the used river sand are 2.44 and 2600 kg/m^3, with a water content of 3.6%. The cement and sand were mixed by using clean tap water according to the mixture proportion, as presented in Table 2. Due to the removal of partial water in cement mortar during the preparation of lined CM, its effective water-cement ratio is 0.35. The external diameter and wall thickness of the used DI pipe are 96mm and 6.5mm, respectively. Table 3 lists the chemical composition of ductile iron, and its microstructure is illustrated in Fig.1.

Table 1. Chemical composition of the used 52.5-grade ordinary Portland cement (wt.%).

Material	SiO_2	Al_2O_3	Fe_2O_3	CaO	MgO	SO_3
Cement	21.1	5.56	3.98	62.48	1.76	2.59

Table 2. Mixture proportion of cement mortar lining of CMLDI pipe.

Sample	water-cement ratio	Mass fraction/%		
		Cement	sand	water
Cement-mortar lining (CM lining)	0.4[*]	100	130	40

[*]Notes: its effective value is 0.35.

Table 3. Chemical composition of ductile iron of CMLDI pipe (wt.%).

Elements	Fe	C	Si	Mn	Mg	P	S	Ti	Cr	Cu	V	Ni
Contents(mass)	92.77	4.02	2.33	0.40	0.2	0.08	0.07	0.03	0.025	0.03	0.035	0.01

2.2 Specimen preparation

The DI pipe was applied for the preparation of specimen, and its internal surface was successively cleaned up by using dilute hydrochloric acid, acetone and purified water. After its internal surface was

completely dried, the mixed CM was lined to the pipe by using the centrifugal method, which is detailed in [6], and the prepared CMLDI pipe is shown in Fig.2.
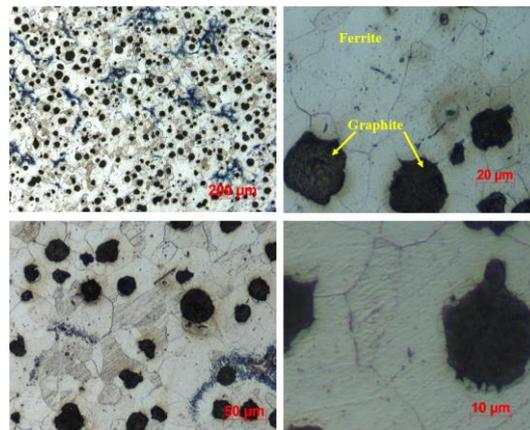
Figure 1. Microstructure of ductile iron of CMLDI pipe
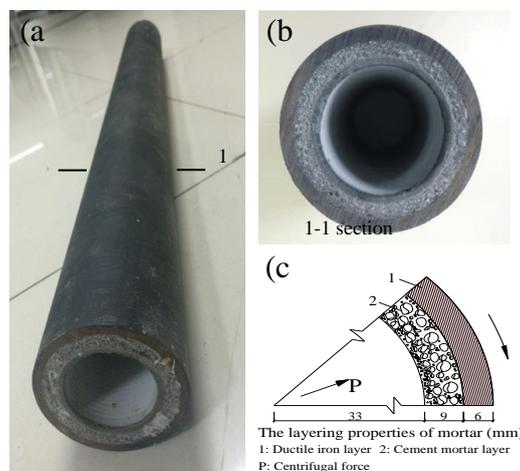
Figure 2. Prepared CMLDI pipe: (a) Completed specimen (b) Cross-sectional view, (c) Stratification

In order to perform the electrochemical measurement on the corrosion process of CMLDI pipe in flowing corrosive solutions, a 10 mm-high circular ring was cut from the prepared CMLDI pipe, and then it was connected with two 250 mm-long copper wires to avoid one of them from failure. Next, the surfaces of circular ring were sealed with the epoxy resin except its internal surface, which was treated as the corrosion face. Finally, the electrochemical specimen was finished, as presented in Fig.3, and the structural parameters of the prepared specimen are shown in Table 4.
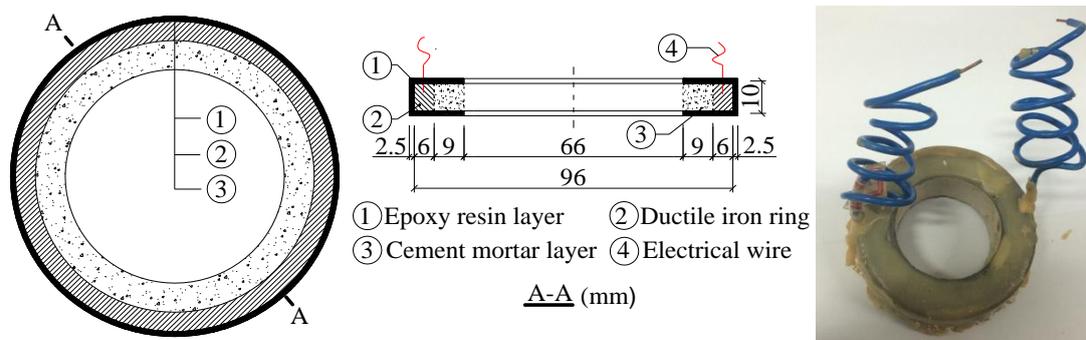
Figure 3. The prepared electrochemical circular ring specimen of CMLDI pipe

Table 4. Structural parameters of the prepared electrochemical specimen of CMLDI pipe

Specimen	Corrosion solutions	Height (mm)	Diameter (mm)		Layer thickness (mm)		
			Inside	Outside	Ductile iron	Cement mortar	Epoxy
OPCO-W	Purified water						
OPCO-N	NH_4NO_3 solution	10	66	96	6	9	2.5
OPCO-Cl	NH_4Cl solution						

2.3 Corrosion solutions and experiment

In the corrosion experiment, purified water, 6M NH_4NO_3 solution and 6M NH_4Cl solution were selected as corrosive solutions. Purified water was utilized to simulate the conventional leaching of the CMLDI pipe in actual water supply. NH_4NO_3 solution was used to accelerate the leaching of lined CM layer [17], but it has no corrosion on the DI pipe. NH_4Cl solution can accelerate the leaching CM lining and the corrosion of DI pipe [18,19]. The reagents of NH_4Cl and NH_4NO_3 with a solubility of 37.2 and 216g/100mL at room temperature were utilized to prepare the corrosive solutions.

In the corrosion experiment, firstly, the prepared specimens were respectively put into three corrosive solutions, including purified water, 6M NH_4NO_3 solution and 6M NH_4Cl solution, which were placed in different plastic tanks. Secondly, the corrosive solution was disturbed by the pump with a power of 12 watts to form the flowing solution with a velocity of 0.5m/s acting on the internal surface of CMLDI specimen. The outlet of pump was 15cm away from the specimen, and exactly opposite its corrosion interface. Finally, the corroded specimen was used to perform the PDP and EIS measurements, as well as to microscopically analyze its chemical composition and microstructural morphology. There were three groups of experimental setups, corresponding to three corrosive solutions placing CMLDI specimens. The schematic diagram of corrosion experiment is shown in Fig.4(a).
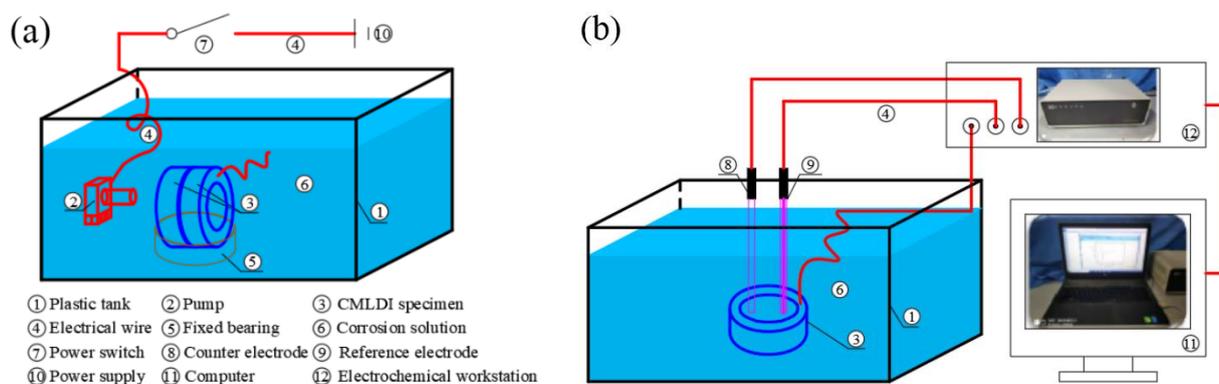
Figure 4. Schematic diagram of corrosion experiment of CMLDI specimen (a) and electrochemical measurements of the corroded CMLDI specimen (b)

2.4 Electrochemical measurements

Electrochemical measurements were performed at room temperature in a conventional three-electrode system. The CMLDI circular ring electrode in Fig.2, the commercial saturated calomel electrode (SCE) and platinum electrode were respectively used as working electrode, reference electrode and counter electrode in the electrochemical measurement system, and its schematic diagram is presented in Fig.4(b). At the immersion time of 0, 30, 60, 90 and 120 days in flowing corrosive solutions, the corroded specimens were put into the system in Fig.4(b) to perform the electrochemical measurements, and their open circuit potential, potentiodynamic polarization and EIS curves were respectively measured by using the electrochemical workstation. A frequency range of 10mHz~100kHz and sinusoidal voltage with an amplitude of ±10 mV were used to conduct the EIS measurement, and the obtained data were analyzed by a fit and simulation procedure of the ZSimpWin software [20]. The PDP measurement was performed by applying a corrosion potential (Ecorr) ranged from -100mV to +150 mV with a scan rate of 0.1 mV/s, and the corrosion current density (icorr) was obtained by the Tafel curve extrapolation method [21].

2.5 Microscopic analysis

After finishing the electrochemical measurements of CMLDI electrode specimens, they were broken to prepare some samples for microscopic analysis, which can investigate the microstructural morphology and chemical composition of lined CM and DI, further revealing the corrosion mechanism of the CMLDI specimens in flowing corrosive solutions [8]. The microscopic analysis was carried out by using X-ray diffractometer (XRD) and Scanning Electron Microscopy (SEM) with the Energy Dispersive X-ray Spectroscopy (EDS). The preparation process of the microscopic samples from the CMLDI electrode specimens is shown in Fig. 5.
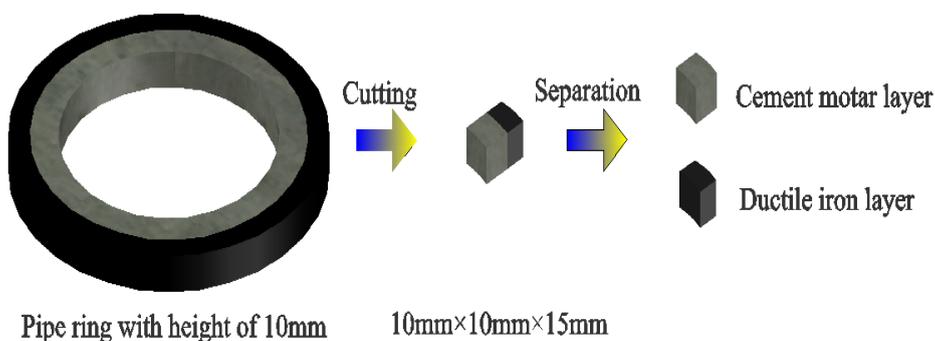
Figure 5. Preparation of microscopic samples from CMLDI electrode specimen

3. RESULTS AND DISCUSSION

3.1. Open circuit potential (OCP)

Fig.6 presents the time-varying open circuit potential (OCP) of CMLDI specimens in different flowing corrosive solutions. It can be obtained from the figure that, the initial OCPs of the specimens OPCO-W, OPCO-N and OPCO-Cl, which are placed in purified water, 6M NH_4NO_3 solution and 6M NH_4Cl solution, are -157, -192 and -277 mV *vs.* SCE, respectively. Their OCPs correspond to no corrosion state, in which the OCP is less than -350 mV *vs.* SCE [14,22]. But, with an increase in immersion time, their OCPs exhibit some different changes. The OCP of OPCO-Cl has a significant shift for the first 60-day immersion, decreasing from the initial -277 to -571.0 mV *vs.* SCE during the first 30-day immersion and then to -725 mV *vs.* SCE for 60-day immersion and finally maintains about -720 mV *vs.* SCE for 120-day immersion. This indicates that, after immersed for 60 days in the flowing 6M NH_4Cl solution, CMLDI specimen reaches to a corrosion state. But for the specimens OCPO-W and OPCO-N, their OCPs have always been fluctuating about the initial values which are less than -350mV *vs.* SCE, indicating that they have basically no corrosion after immersed for 120 days in flowing purified water and 6M NH_4NO_3 solution.
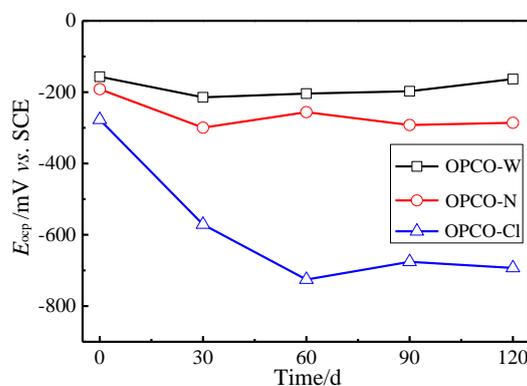
Figure 6. Time-varying OCP of the specimens OPCO-W, OPCO-N and OPCO-Cl in flowing corrosive solutions

3.2. Potentiodynamic polarization (PDP)

Fig.7 shows the potentiodynamic polarization curves of CMLDI specimens at different immersion time. It is known from the figure that, after 120 days of immersion, there occurs an obvious negative shift in the corrosion potential, E_{corr}, of the specimen OPCO-Cl, but the corrosion potentials of OCPO-W and OPCO-N fluctuate in the range of -191.79~-299.70 mV *vs.* SCE. Generally speaking, a high negative shift of E_{corr} indicates a high corrosion degree [23], so the OPCO-Cl is more premature corrosion than OCPO-W and OPCO-N.
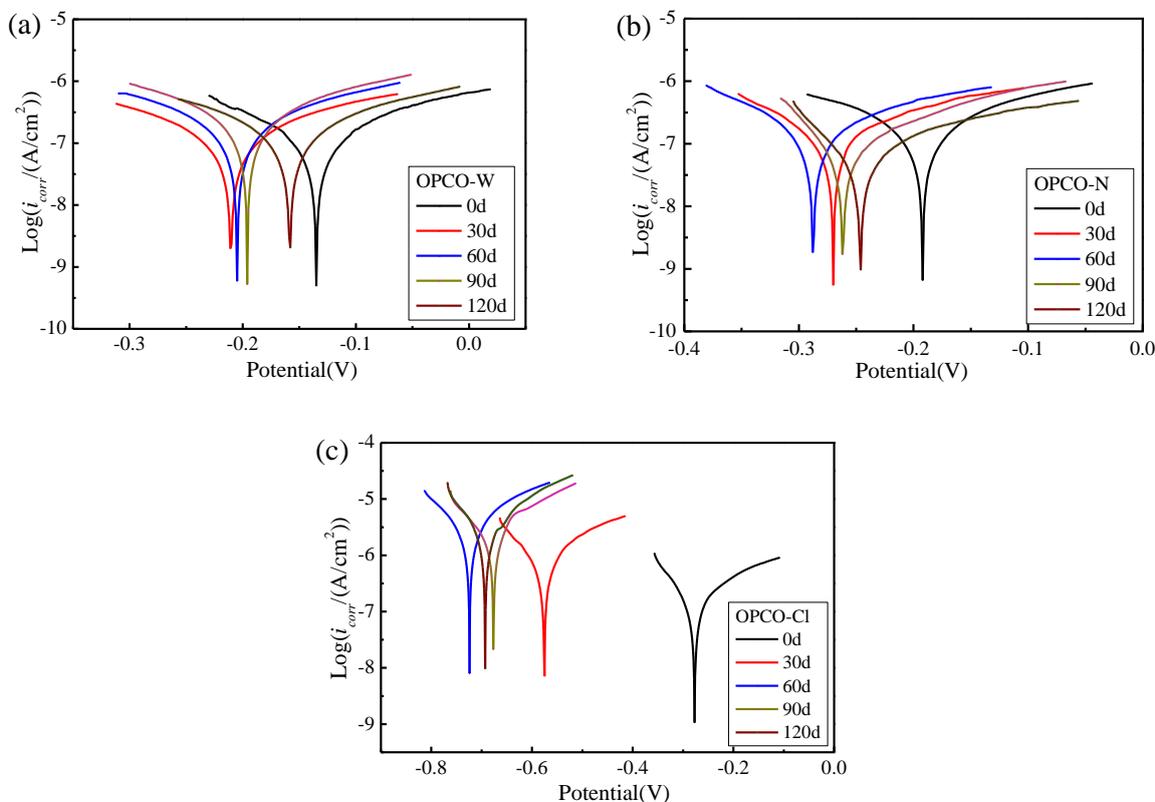
Figure 7. Potentiodynamic polarization curves of the specimens OPCO-W (a), OPCO-N (b) and OPCO-Cl (c) at different immersion time

In order to further describe the corrosion characteristics of CMLDI specimens in flowing corrosive solutions, the corrosion current densities and polarization resistances of the specimen, i_{corr} and R_p, are respectively determined by the extrapolation method and the Stern-Geary relationship [24], as listed in Table 5. Here, $R_p = B/i_{corr}$, and B is the Stern-Geary constant, which is 26mV in the active state and 52 mV in the passive state, respectively, and it can be obtained by the measured anodic Tafel slope β_a and cathodic Tafel slope β_c

$$B = \frac{\beta_a \times \beta_c}{2.303(\beta_a + \beta_c)} \qquad (1)$$

It is known from Table 5 that, during 120-day immersion in flowing purified water, the polarization resistance and corrosion current density of the specimen OPCO-W basically maintain 200 $k\Omega \cdot cm^2$ and $0.16\mu A \cdot cm^{-2}$, respectively. The corrosion current density is obviously lower than the

corrosion threshold, $0.2\mu A \cdot cm^{-2}$ [6,25]. Thus, the corrosion has not occurred on the specimen OPCO-W in the flowing purified water.

In flowing 6M NH_4NO_3 solution for 120 days, the polarization resistance of OPCO-N decreases from 209.5 to $180.8\ k\Omega \cdot cm^2$, but its corrosion current density is about $0.15\mu A \cdot cm^{-2}$, which is similar to that in purified water. The reason for this result is that, the leaching process of CM in 6M NH_4NO_3 solution is about 130 times of that in purified water [26], and fast leaching results in great increase in the porosity of lined CM, which can reduce its resistance. However, the nitrate ion in the solution has no corrosion on DI, so the resistance of DI surface has basically no change, and its corrosion current density is very small. The reduction in the polarization resistance of OPCO-N is mainly caused by the resistance reduction of the CM lining, which is far less than the resistance of DI surface [27].

For the specimen OPCO-Cl, its R_p decreases from 195.3 to $10.0\ k\Omega \cdot cm^2$ during the first 60-day immersion, and then reduces to $5.3\ k\Omega \cdot cm^2$ for 120-day immersion. Meanwhile, its corrosion current density increases with immersion time, and reaches to 2.81 and $4.20\ \mu A \cdot cm^{-2}$ for 60-day and 120-day immersion, respectively, which are obviously higher than the corrosion threshold, $0.2\mu A \cdot cm^{-2}$. There observe an obvious decrease in polarization resistance and significant increase in corrosion current density, which can indicate that there occur the leaching of CM lining and depassivated corrosion of DI surface in the specimen OPCO-Cl.

Table 5. Electrochemical parameters of the specimens OPCO-W, OPCO-N and OPCO-Cl at different immersion time obtained from PDP measurement

Specimens	Immersion time (day)	i_{corr} ($\mu A/cm^2$)	β_a (mV/dec)	β_c (mV/dec)	R_p ($k\Omega \cdot cm^2$)
OPCO-W	0	0.15	126	173	211.3
	30	0.17	151	162	199.2
	60	0.18	147	171	190.4
	90	0.20	156	193	187.2
	120	0.19	133	218	188.4
OPCO-N	0	0.18	164	185	209.5
	30	0.16	113	242	208.4
	60	0.17	119	197	189.9
	90	0.14	96	205	202.2
	120	0.15	80	282	180.8
OPCO-Cl	0	0.12	83	155	195.3
	30	0.63	116	188	49.5
	60	2.81	106	164	10.0
	90	3.70	98	211	7.9
	120	4.20	77	163	5.3

3.3 Electrochemical impedance spectra (EIS)

Fig.8 show the Nyquist curves of specimens OPCO-W, OPCO-N and OPCO-Cl at different immersion time. It can be obtained from the figures that, two capacitance arcs can be observed from the

Nyquist curve of every specimen, which can respectively characterize the electrochemical characteristics of CM lining and the DI surface.

It can be obtained from Fig.8(a) that, the Nyquist curve of OPCO-W in flowing purified water remains basically unchanged with immersion time. In the low frequency region, the capacitive arcs always maintain large slopes, which indicates a passive state of DI surface [28]. Thus, the CM lining and DI surface have basically no corrosion, which is in agreement with the results from the potentiodynamic polarization measurement.
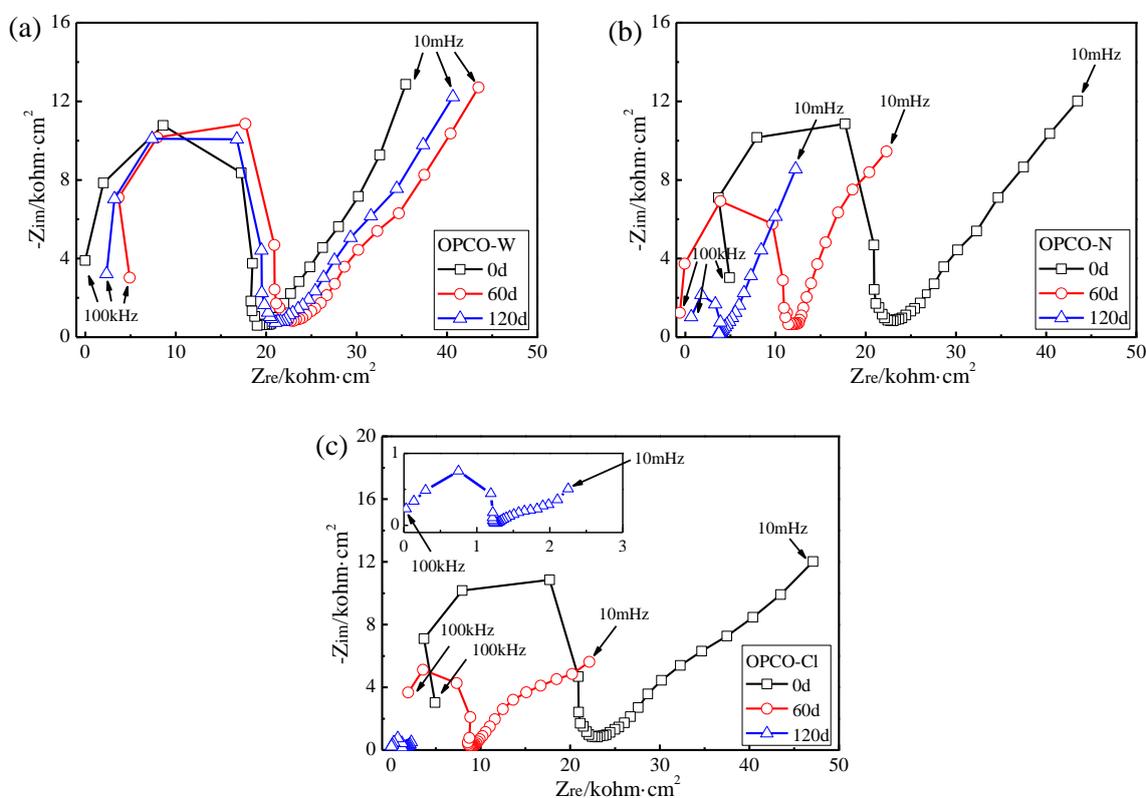
Figure 8. Nyquist curves of the specimens OPCO-W (a), OPCO-N (b) and OPCO-Cl (c) at different immersion time

It is known from Fig.8(b) that, in the high frequency region, the Nyquist curve of OPCO-N in flowing NH_4NO_3 solution has a reduction in the diameter of capacitive arc with immersion time, but in its low frequency region, the slope of capacitive arc has basically no change. This indicates that the resistance of CM lining in OPCO-N has a significant decrease with immersion time, but the resistance of DI surface is basically unchanged. Therefore, the CM lining of OPCO-N has an obvious leaching, causing an increase in its porosity, but its DI surface has basically no corrosion, which is similar to that in flowing purified water.

It can be seen from Fig.8(c) that, the Nyquist curve of OPCO-Cl in flowing NH_4Cl solution has an obvious change with immersion time. In the high and low frequency regions, the diameter of two capacitive arcs has a significant reduction, which indicates that the CM lining and DI surface of OPCO-Cl have a severe leaching and corrosion.

In order to further characterize the corrosion behavior of CMLDI pipe, the experimental data obtained from the EIS measurement can be fitted by the equivalent circuits with two time constants [22], as shown in Fig.9. In Fig.9, R_s is the solution resistance, R_c is the resistance of CM lining, R_{ct} is the charge transfer resistance of DI surface, C_c and Q_{dl} are the capacitance of double-layer capacitors associated with the solution-CM and CM-DI interfacial zones, respectively, W is the Warburg impedance. R_c and R_{ct} are used to characterize the corrosion characteristics of both CM lining and DI surface, which can describe the leaching behavior of CM lining and the depassivation process of DI surface in three corrosive solutions, respectively. According to the equivalent circuits, the R_c, R_{ct} and Q_{dl} of specimen are obtained by using the ZSimpWin software, as listed in Table 6.
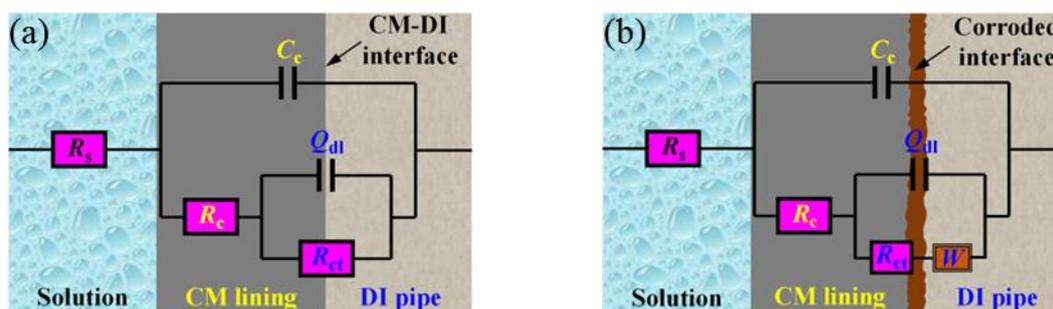
Figure 9. The equivalent circuits of passive CM-DI interface (a) and depassivated CM-DI interface (b)

Table 6. Fitting electrochemical parameters of CMLDI specimens at different immersion time according to the equivalent circuits

Number of Specimen	Immersion time T(day)	Solution resistance $R_s/(\Omega \cdot cm^2)$	Lining resistance $R_c/(k\Omega \cdot cm^2)$	Double-layer capacitor $Q_{dl}/(\mu F \cdot cm^{-2})$	Charge trans. resistance $R_{ct}/(k\Omega \cdot cm^2)$	Capacitor parameter n	Warburg impedance $W/(\Omega^{-1} \cdot cm^{-2} \cdot S^{1/2})$
	0	5.89	21.89	40.61	200.45	0.92	—
OPCO-W	60	9.61	21.64	44.68	179.47	0.89	—
	120	6.33	20.87	48.32	184.33	0.90	—
	0	9.87	21.79	42.54	193.14	0.92	—
OPCO-N	60	7.15	12.46	47.53	186.45	0.91	—
	120	7.33	2.83	49.87	178.09	0.88	—
	0	8.90	21.67	41.91	192.15	0.91	—
OPCO-Cl	60	4.31	4.66	130.45	8.89	0.74	0.00107
	120	2.54	2.13	156.34	3.16	0.73	0.00104

It is known from Table 6 that, after 120 days of immersion in flowing purified water, the R_c of CM lining and R_{ct} of DI surface of specimen OPCO-W are basically unchanged, indicating that OPCO-W is no corrosion in purified water. In flowing NH_4NO_3 solution, the R_c of CM lining in the OPCO-N decreases from about 21.79 to 2.83 $k\Omega \cdot cm^2$ after 120 days of immersion, while the R_{ct} of DI surface in the OPCO-N basically maintain about 185 $k\Omega \cdot cm^2$, which is similar to that of the OPCO-W. Thus, an obvious calcium leaching of CM lining occurs in the OPCO-N. But in flowing NH_4Cl solution, there

occur an obvious reduction in the R_c of CM lining and R_{ct} of DI surface in the OPCO-Cl, which indicate that the CM lining and DI surface of the specimen OPCO-Cl have a severe corrosion, respectively.

Additionally, the Q_{dl} can also characterize the corrosion degree of the DI surface, and higher corrosion degree results in greater roughness of DI surface, which produces more deviation of the Q_{dl} on the DI surface from the ideal capacitor. The DI surface is in a passive state when its Q_{dl} is less than 100 $\mu F \cdot cm^{-2}$, otherwise it is in a depassivated state [6]. It is known from Table 6 that, after 120 days of immersion, the Q_{dl} of OPCO-W and OPCO-N is lower than 50 $\mu F \cdot cm^{-2}$, which indicates that the DI surface remains in a passive state in flowing purified water and NH_4NO_3 solution. But, the Q_{dl} of OPCO-Cl is more than $100\mu F \cdot cm^{-2}$ after 60 days of immersion, so the corrosion degree of the CMLDI specimen in flowing NH_4Cl solution is obviously greater than that of the specimens in flowing purified water and NH_4NO_3 solution.

3.6 Microscopic analysis

3.6.1 SEM/EDS

In order to further reveal the corrosion mechanism of CMLDI pipe, the electrochemical specimens immersed in corrosive solutions for 120 days, OPCO-W, OPCO-N and OPCO-Cl, were broken to prepare SEM/EDS samples. These samples are used to observe the microstructure morphology and analyzing the chemical composition of the CM-DI interfacial zone. Fig.10 presents the surface state of ductile iron samples in different flowing corrosive solutions. It is known from the figure that, an obvious corrosion layer like reddish-brown rusts can be observed on the DI surface of OPCO-Cl, and its volume expansion causes the reduction in cohesiveness and further separation of CM-DI interface zone [29]. But, the DI surfaces of OPCO-W and OPCO-N have basically no corrosion, and some left CM are still well attached to the DI surface after peeling off the CM lining, indicating a good cohesiveness of CM-DI interface.

Fig.11 gives the microstructural morphology and chemical composition of CM-DI interfacial zone in the specimens OPCO-W, OPCO-N and OPCO-Cl immersed in flowing corrosive solutions for 120 days, respectively. It is known from Fig.11(a) that, at the CM-DI interfacial zone of OPCO-Cl, some loose corrosion products are obviously observed on the DI surface, while its chemical compositions mainly includes iron and oxygen as well as a little carbon and chlorine. Compared with the chemical composition of DI in Table 3, there occurs a decrease in iron content and an increase in oxygen content, which indicates the formation of rust at the CM-DI interfacial zone [30], which further shows that the DI surface of OPCO-Cl has been corroded. It is seen from Fig.11(b) and (c), at the CM-DI interfacial zone of OPCO-W and OPCO-N, their microstructural morphology and chemical compositions can clearly be found, and they have obvious difference with that of OPCO-Cl. Furthermore, there observes a compact microstructure containing calcium hydroxide and C-S-H gel at the CM-DI interfacial zone of OPCO-W [31]. But the microstructure at the CM-DI interfacial zone of OPCO-N is loose and porous, and no calcium hydroxide is observed [32]. Additionally, the interfacial zone of OPCO-W and OPCO-N includes the bonded CM and exposed DI, and there contains mainly calcium and oxygen in the bonded CM, in which the calcium content is respectively 36.32% and 21.71% in the OPCO-W and OPCO-N.

This indicates that the leaching degree of CM lining of the specimen OPCO-N in NH_4NO_3 solution is greater than that of the OPCO-W in the purified water. But there contains mainly iron and carbon on the surface of exposed DI, which is basically the same as the initial composition of DI, indicating no corrosion of DI at the interfacial zone in the OPCO-W and OPCO-N, as seen in Fig.11(b) and (c).
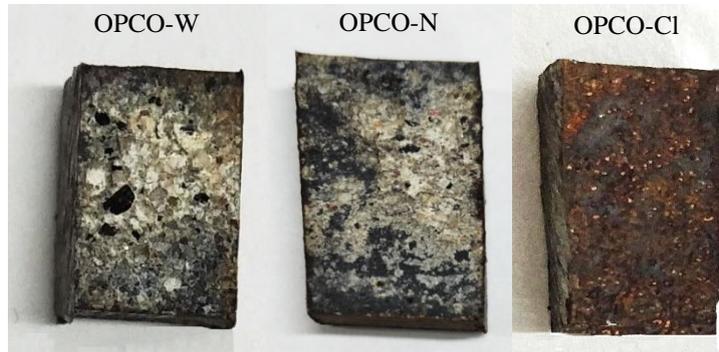
Figure 10. Surface state of DI samples from CMLDI specimen in different flowing corrosive solutions for 120 days
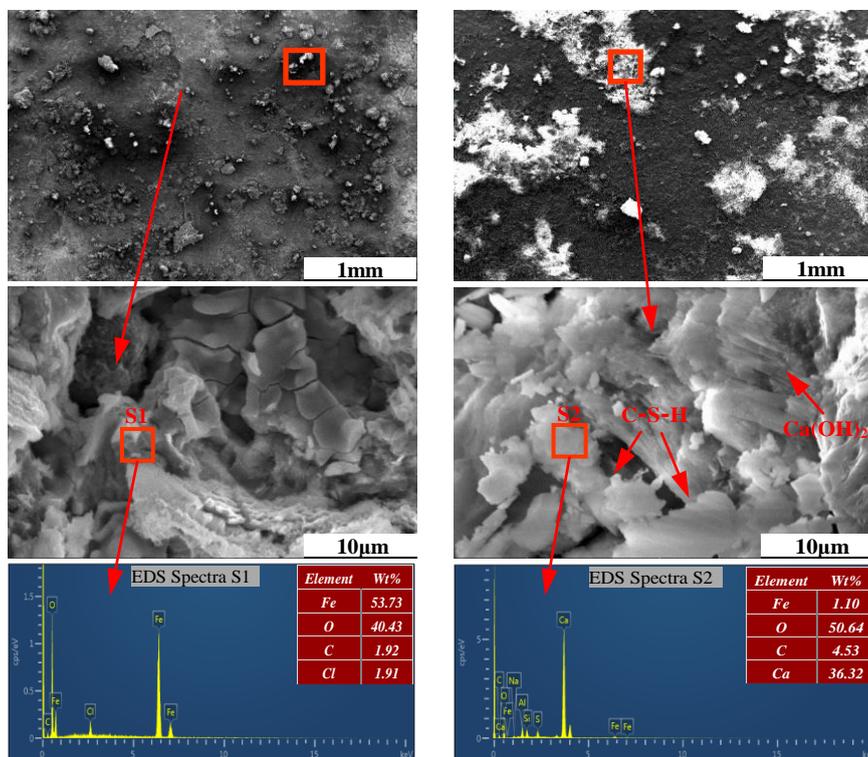
(a) Specimen OPCO-Cl   (b) Specimen OPCO-W
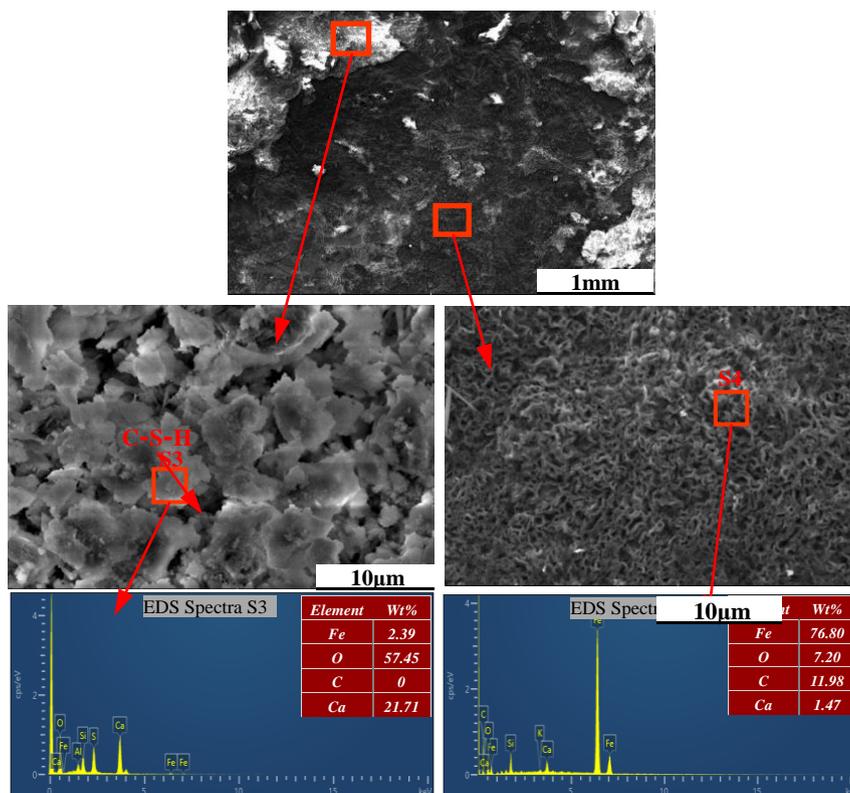
(c) Specimen OPCO-N

Figure 11. Microstructural morphology and chemical composition of CM-DI interfacial zone in the specimens OPCO-W, OPCO-N and OPCO-Cl in flowing corrosive solutions for 120 days

3.6.2 XRD

The change of phase composition can reflect the leaching characteristics of CM lining caused by corrosive solution [33]. In the accelerated leaching experiments, the flowing corrosive solution has an important influence on the leaching characteristics of CM lining in CMLDI pipe. In order to analyze the influence of corrosive solution on the phase composition in the CM lining of CMLDI pipe specimen, Fig.12 presents the XRD pattern of samples from the CM lining of the OPCO-W, OPCO-N and OPCO-Cl specimens after 120 days of immersion, and the peak intensity ratio for crystallographic planes of the phases in the samples is listed in Table 7. It can be obtained from Fig.12 and Table 7 that, there observe obvious diffraction peaks of $Ca(OH)_2$, C-S-H and C-A-S-H gel phases in the sample of OPCO-W. But in the samples of OPCO-N and OPCO-Cl, there are no diffraction peaks for (001), (101), (102) and (110) crystallographic planes of $Ca(OH)_2$ at $2\theta = 18.0°$, $34.1°$, $47.1°$ and $50.8°$, but the diffraction peaks of C-S-H and C-A-S-H gel can be still observed. In addition, the intensity of diffraction peaks of C-S-H gel in the sample of OPCO-W is slightly higher than that in the samples of OPCO-N and OPCO-Cl. The XRD results show that, the CM lined in the OPCO-W has basically no calcium leaching [34], but calcium hydroxide has been fully leached in the CM lined in the OPCO-N and OPCO-Cl. Thus, in the flowing NH_4NO_3 solution and NH_4Cl solution for 120 days, there has an obvious calcium leaching in the CM lining, which is far faster than that in the purified water [35].
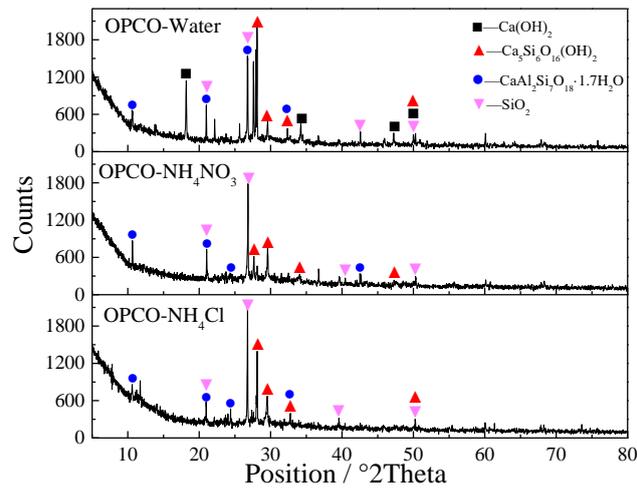
Figure 12. XRD patterns of the samples from CM lining of the specimens OPCO-W, OPCO-N and OPCO-Cl in corrosive solutions for 120 days

Table 7. Peak intensity ratio for crystallographic planes of CM lining of CMLDI specimens in different flowing corrosive solutions for 120 days

Phases	Parameter	Specimens											
		OPCO-W				OPCO-N				OPCO-Cl			
$Ca(OH)_2$	Planes	(001)	(101)	(102)	(110)	—	—	—	—	—	—	—	—
	I/I_{max}	72	100	30	31	—	—	—	—	—	—	—	—
CSH gel	Planes	(013)	(111)	(200)	(302)	(013)	(111)	(015)	(302)	(013)	(111)	(200)	(302)
	I/I_{max}	19	100	18	12	19	100	2	12	19	100	18	12
CASH gel	Planes	(020)	(040)	(401)	(060)	(020)	(040)	(240)	(701)	(020)	(040)	(401)	(060)
	I/I_{max}	100	60	6	35	100	60	35	30	100	60	6	35
SiO_2	Planes	(100)	(101)	(200)	(112)	(100)	(101)	(200)	(112)	(100)	(101)	(102)	(112)
	I/I_{max}	16	100	6	13	22	100	6	14	16	100	8	13

4. CONCLUSIONS

This paper investigated the corrosion characteristics of CMLDI pipe in flowing purified water, 6M NH_4NO_3 solution and 6 M NH_4Cl solution by using electrochemical measurement and microscopic analysis. Some DI pipe specimens lined with CM were prepared, and their corrosion characteristics in three flowing corrosive solutions were analyzed by electrochemical measurements, including OCP, PDP and EIS. Meanwhile, the microstructure morphology of CM-DI interfacial zone and phase composition of CM lining of CMLDI pipe in flowing corrosive solutions for 120 days were respectively characterized by SEM/EDS and XRD. The following conclusions can be drawn:

In flowing purified water, there has no obvious change in the resistance of CM lining, the charge transfer resistance of DI surface and the corrosion current density of CMLDI pipe specimen, and calcium hydroxide can be clearly observed on the lined CM. The CMLDI pipe specimen has no obvious corrosion in flowing purified water for 120 days.

In flowing 6M NH_4NO_3 solution, there is a significant decrease in the resistance of the CM lining of CMLDI specimen, but basically no change in the charge transfer resistance and corrosion current

density of its CM-DI interfacial zone. Microscopically, no calcium hydroxide can be found in the lined CM, and some loose microstructure of CM and exposed DI can be observed at the CM-DI interfacial zone of CMLDI pipe specimen. The CM lining of CMLDI pipe specimen has an obvious calcium leaching, but its DI surface has no corrosion.

However, in flowing 6M NH_4Cl solution, there has an obvious decrease in the resistance of CM lining and the charge transfer resistance of the DI surface in the CMLDI pipe specimen, and its corrosion current density is greater than the corrosion threshold. Additionally, the CM lining is fully separated from the DI of CMLDI pipe specimen, and its CM-DI interfacial zone only contains corrosion production of DI, while no calcium hydroxide is observed in the separated CM lining. Severe corrosion occurs on the CM lining and DI surface of the CMLDI pipe specimen immersed for 120 days in flowing 6M NH_4Cl solution.

References

1. S.A.S. El-Hemaly, H.A.M. Abdallah, M.F. Abadir and H.H. El Sersy, *Mater. Des.*, 29 (2008) 1280.
2. N.A. Barton, T.S. Farewell, S.H. Hallett and T.F. Acland, *Water Res.*, 164 (2019) 114926.
3. H.J. Kocks and W. Siedlarek, *Mater. Corros.*, 53 (2002) 546.
4. X.H. Sun, X.B. Zuo, G.J. Yin, K. Jiang and Y.J. Tang, *Constr. Build. Mater.*, 150 (2017) 703.
5. J. Jain and N. Neithalath, *Cem. Concr. Compos.*, 31 (2009) 176.
6. S. Zou, X.B. Zuo, A.F. Abubakar, S.L. He and W.Y. Huang, *Constr. Build. Mater.*, 193 (2018) 1.
7. X.B. Zuo, X.N. Li, Z.Y. Liu, W.Y. Huang and X.H. Sun, *Constr. Build. Mater.*, 229 (2019) 116907.
8. Y.R. Song, Y.M. Tian, X. Zhao, H. Guo and H.Y. Zhang, *Int. J. Electrochem. Sci.*, 11 (2016) 7031.
9. H.H. Hu, X.B. Zuo, D. Cui and Y.J. Tang, *Constr. Build. Mater.*, 224 (2019) 762.
10. P. Feng, C.W. Miao and J.W. Bullard, *Cem. Concr. Compos.*, 49 (2014) 9.
11. K. Kurumisawa, K. Haga, D. Hayashi and H. Owada, *Phys. Chem. Earth.*, 99 (2017) 175.
12. H.W. Wu, K.Y. Pan, Y. Dai, H.S. Jin and F.H. Li, *Int. J. Electrochem. Sci.*, 14 (2019) 4995.
13. B. Lin, Y. Zuo, Y.M. Tang, X.H. Zhao and P. Rostron, *Int. J. Electrochem. Sci.*, 14 (2019) 3081.
14. C.Q. Ye, R.G. Hu, S.G. Dong, X.J. Zhang, R.Q. Hou, R.G. Du, C.J. Lin and J.S. Pan, *J. Electroanal. Chem.*, 688 (2013) 275.
15. J.J. Shi, J. Ming and W. Sun, *Cem. Concr. Compos.*, 92 (2018) 110.
16. C.R. Das, C. Ravishankar, S.K. Albert, S.A Krishnan., A. Moitra, K.V. Rajkumar and A.K. Bhaduri, *Eng. Fail. Anal.*, 92 (2018) 456.
17. A.M. Forster, E.M. Szadurski and P.F.G. Banfill, *Constr. Build. Mater.*, 72 (2014) 199.
18. U.M. Angst, B. Elsener, C.K. Larsen and Ø. Vennesland, *Corros. Sci.*, 53 (2011) 1451.
19. Z.J. Song, L.H. Jiang and H.Q. Chu, *Constr. Build. Mater.*, 153 (2017) 211.
20. Z.Q. Bai, Z.F. Yin, D. Wei, X.F. Wang and C.X. Yin, *Mater. Corros.*, 61 (2010) 689.
21. M.A. Amin, K.F. Khaled and S.A. Fadl-Allah, *Corros. Sci.*, 52 (2010) 140.
22. A.A. Hermas and M.S. Morad, *Corros. Sci.*, 50 (2008) 2710.
23. J.J. Shi, D.Q. Wang, J. Ming and W. Sun, *J. Mater. Civ. Eng.*, 30 (2018) 04018042.
24. A. Poursaee, *Cem. Concr. Res.*, 40 (2010) 1451.
25. P.V. Nygaard and M.R. Geiker, *Mater. Corros.*, 63 (2012) 200.
26. K.S. Wan, Y. Li and W. Sun, *Constr. Build. Mater.*, 40 (2013) 832.

27. J. Gulikers, *Mater. Corros*., 56 (2005) 393.
28. M. Liu, X.Q. Cheng, X.G. Li, Z. Jin and H.X. Liu, *Constr. Build. Mater*., 93 (2015) 884.
29. Y.X. Zhao, H.Y. Ren, H. Dai and W.L. Jin, *Corros. Sci*., 53 (2011) 1646.
30. J.J. Shi, D.Q. Wang, J. Ming and W. Sun, *J. Mater. Civ. Eng*., 30 (2018) 04018232.
31. F.H. Han, R.G. Liu and P.Y. Yan, *Constr. Build. Mater*., 68 (2014) 630.
32. X.B. Zuo, Y.J. Tang, G.J. Yin, K. Jiang and S.L. He, *J. Mater. Civ. Eng*., 29 (2017) 04017187.
33. K. Haga, S. Sutou, M. Hironaga, S. Tanaka and S. Nagasaki, *Cem. Concr. Res*., 35 (2005) 1764.
34. Y.J. Tang, X.B. Zuo, G.J. Yin, S.L. He and O. Ayinde, *Mater. Des*., 114 (2017) 612.
35. T.P. Quoc, N. Maes, D. Jacques, J. Perko, G. De Schutter and G. Ye, *Constr. Build. Mater*., 115 (2016) 179.